Available online at www.sciencedirect.com
SCIENCE DIRECT®
Journal of Organometallic Chemistry 690 (2005) 5036–5048
Journal of Organometallic Chemistry
www.elsevier.com/locate/jorganchem

# Evolution of lowest singlet and triplet excited states with transition metals in group 10–12 metallaynes containing biphenyl spacer

Li Liu [a,b], Suk-Yue Poon [a], Wai-Yeung Wong [a,*]

[a] *Department of Chemistry and Centre for Advanced Luminescence Materials, Hong Kong Baptist University, Waterloo Road, Kowloon Tong, Hong Kong, PR China*

[b] *Faculty of Chemistry and Material Science, Hubei University, Wuhan 430062, PR China*

Received 28 January 2005; received in revised form 17 February 2005; accepted 17 February 2005
Available online 17 March 2005

**Abstract**

A new series of thermally stable group 10 platinum(II) and group 12 mercury(II) poly-yne polymers containing biphenyl spacer *trans*-[–Pt($PBu_3$)$_2$C≡C(*p*-$C_6H_4$)$_2$C≡C–]$_n$ and [–HgC≡C(*p*-$C_6H_4$)$_2$C≡C–]$_n$ were prepared in good yields by Hagihara's dehydrohalogenation reaction of the corresponding metal chloride precursors with 4,4′-diethynylbiphenyl HC≡C(*p*-$C_6H_4$)$_2$C≡CH at room temperature. We report the optical spectroscopy of these polymetallaynes and compare the results with their bimetallic model complexes *trans*-[Pt(Ph)($PEt_3$)$_2$C≡C(*p*-$C_6H_4$)$_2$C≡CPt(Ph)($PEt_3$)$_2$] and [MeHgC≡C(*p*-$C_6H_4$)$_2$C≡CHgMe] as well as the group 11 gold(I) counterpart [($PPh_3$)AuC≡C(*p*-$C_6H_4$)$_2$C≡CAu($PPh_3$)]. The structural properties of all model complexes have been studied by X-ray crystallography. The influence of the heavy metal atom in these metal alkynyl systems on the intersystem crossing rate and the spatial extent of lowest singlet and triplet excitons is systematically characterized. Our investigations indicate that the organic triplet emissions can be harvested by the heavy-atom effect of group 10–12 transition metals (viz., Pt, Au, and Hg) which enables efficient intersystem crossing from the $S_1$ singlet excited state to the $T_1$ triplet excited state.


*Keywords:* Transition metal; Acetylide; Biphenyl; Crystal structures; Triplet emission

## 1. Introduction

There is a continuing interest in the scientific community in the search for new organic and metal-organic molecular functional materials that could help to sustain the growth of photonic research [1]. In particular, conjugated polymers and their metallated derivatives show a wide domain of intriguing properties useful for the development of optoelectronic devices such as organic light-emitting diodes (OLEDs) [2], photovoltaic cells [3], field-effect transistors [4], sensors [5], and nonlinear optical systems [6]. In fact, harvesting of triplet excitons using metal-containing complexes is still one of the most promising ways of making higher efficiency OLEDs [7]. Among these, rigid-rod organometallic poly-ynes of late transition metals represent an important class of new materials for basic and applied research [8]. Strong spin–orbit coupling induced by a heavy-atom effect mixes the singlet and triplet excited states through efficient intersystem crossing (ISC) so that phosphorescence (or triplet emission) can be measured readily using optical methods. Another attractive feature of this class of metal-containing poly-ynes is that there is great scope for chemical modification of the conjugated units. For these two reasons, this family of metal poly-ynes provides an excellent model system to study directly the relationship between chemical structure and the

* Corresponding author. Tel.: +852 34117074; fax: +852 34117348.
*E-mail address:* rwywong@hkbu.edu.hk (W.-Y. Wong).

0022-328X/$ - see front matter © 2005 Elsevier B.V. All rights reserved.
doi:10.1016/j.jorganchem.2005.02.025

evolution of singlet and triplet excitons [9]. Within this framework, group 10 metal alkynyls and related polymers have been studied extensively in view of their interesting photoluminescence and electronic properties, which depend on the transition metal, the organic ligand, the central spacer in the main chain and the symmetry of the molecules [9].

Recently, there has been a great deal of experimental and theoretical attention focusing on the energy levels of singlet and triplet states in conjugated polymers. To study the triplet excitons directly, we and others have paid much attention to polyplatinynes and their monomers to obtain a clear picture of the spatial extent of the singlet and triplet states and their relative positions strongly influence the ISC rate into the triplet manifold [8,9]. For organic systems, this provides a major nonradiative decay mechanism and reduces the luminescence efficiency. Recently, the energy gap law has been established for triplet states in Pt-containing conjugated polymers and monomers where the intersystem crossing rate depends exponentially on the energy gap to the nearest triplet excited state [9a]. It would be very crucial to understand the factors that control the spatial extent of the singlet and triplet energy levels for the chemical tailoring of the singlet–triplet gap. As continuation of our research efforts in this growing field, we report here a series of group 10–12 metal di-ynes and poly-ynes containing the biphenyl spacer. The X-ray crystal structures of the binuclear model complexes are also described. Although there are many reports on Pt(II) poly-yne systems with a variety of organic spacers, relatively little is known for research studies dealing with variation of metal groups in metallated di-ynyl and poly-ynyl assemblies. Until recently, work has proliferated in the metal-triggered phosphorescent emissions seen in some gold(I)- and mercury(II)-containing metallaynes [10]. The aim of the present investigation is to establish in what way the coordination of various heavy metal groups affects the optical and electronic properties of the metal poly-ynes. The influence of the metal on the nature of the lowest singlet and triplet excited states will be characterized, which is of pivotal importance for understanding the mechanisms of LEDs based on conjugated polymers and thereby improving their macroscopic characteristics.

## 2. Results and discussion

### 2.1. Synthesis

All the metal alkynyl complexes and polymers were obtained in good yields by the general reaction routes described in Scheme 1. The binuclear complexes can be considered the molecular models and the building blocks of long chain organometallic polymers. In the shortform of each formula, the triple bonds are abbreviated by T, and biphenyl by BP. Model monomer complexes and polymers are differentiated by use of the subscripts 1 and $\infty$, respectively. Organic ligand [H–T(BP)T]$_1$ was chosen as a versatile synthon in the present study to form a series of group 10–12 metal acetylide complexes and polymers by adaptation of the dehydrohalogenation procedures reported in the literature [9,11,12]. [Pt–T(BP)T]$_1$ and [Pt–T(BP)T]$_\infty$ were synthesized by CuI-catalyzed dehydrohalogenating coupling of *trans*-[$PtCl_2(PBu_3)_2$] or *trans*-[$PtCl(Ph)(PEt_3)_2$] with 4,4′-diethynylbiphenyl at room temperature (r.t.). The feed mole ratios of the platinum chloride precursors and the diethynyl ligand were 2:1 and 1:1 for the model complex and polymer syntheses, respectively, and each product was carefully purified to remove ionic impurities and catalyst residues. The diplatinum complex [Pt–T(BP)T]$_1$ was isolated by preparative TLC on silica. Purification of the polymer [Pt–T(BP)T]$_\infty$ was accomplished by silica column chromatography using $CH_2Cl_2$ as the eluent and it was obtained in high purity. Mercuration of [H–T(BP)T]$_1$ with a stoichiometric quantity of $HgCl_2$ using methanolic NaOH at r.t. gave an off-white solid identified as [Hg–T(BP)T]$_\infty$ [10d]. Complex [Hg–T(BP)T]$_1$ was also synthesized by treatment of [H–T(BP)T]$_1$ with two equivalents of MeHgCl, in which one coordination site is protected by a Me group, under similar basic medium [11]. Likewise, we have also prepared the $d^{10}$ digold(I) diacetylide counterpart [Au–T(BP)T]$_1$, an isoelectronic and isolobal analog of [Hg–T(BP)T]$_1$, by reaction of $Au(PPh_3)Cl$ with [H–T(BP)T]$_1$ in a mole ratio of 2:1 in the presence of a base [12]. The yields of these transformations are high in each case. All the new complexes and polymers are air-stable and can be stored without demanding any special precautions. They generally exhibit good solubility in chlorocarbons such as $CH_2Cl_2$ and $CHCl_3$, but are insoluble in hydrocarbons. However, we note that only the lower molecular-weight fraction of [Hg–T(BP)T]$_\infty$ and [Pt–T(BP)T]$_\infty$ can readily dissolve in chlorinated solvents and there is always some insoluble portion left in the solution (presumably consisting of polymer chains of very high molecular weights) which requires filtration prior to characterization. Estimates of the molecular weights using gel permeation chromatography (GPC) in THF indicate that the degrees of polymerization calculated from $M_n$ are 16 and 6 for [Pt–T(BP)T]$_\infty$ and [Hg–T(BP)T]$_\infty$ (soluble oligomer portion), respectively. The GPC-values should be used with great care and the GPC method does not give absolute values of molecular weights but provides a measure of hydrodynamic volume. Rod-like polymers in solution possess different hydrodynamic properties than flexible polymers. So, calibration of the GPC with polystyrene standards is likely to inflate the values of the molecular weights of the polyynes to some extent.

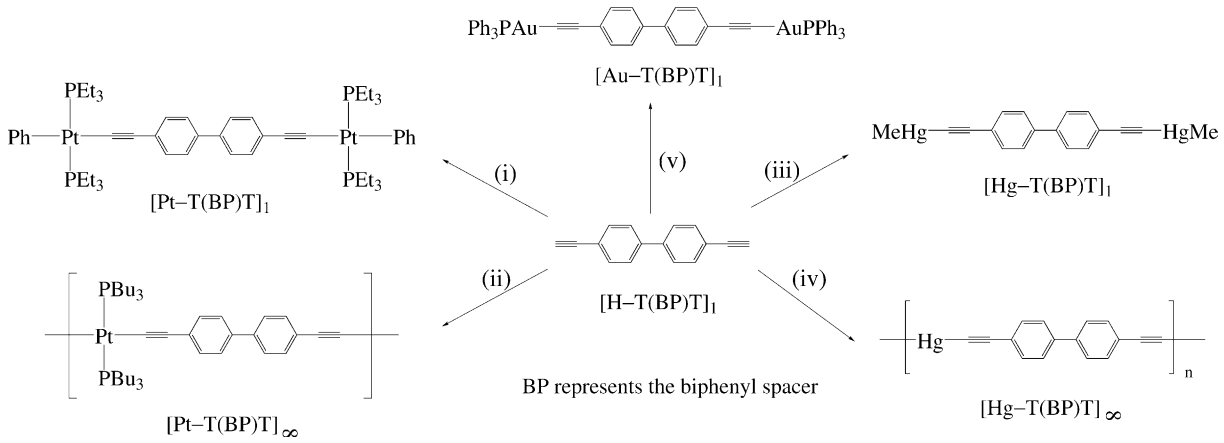


Scheme 1. (i) *trans*-[PtPh(Cl)($PEt_3$)$_2$], CuI, $^iPr_2NH$, r.t.; (ii) *trans*-[$PtCl_2(PBu_3)_2$CuI, $^iPr_2NH$, r.t.; (iii) MeHgCl, NaOH/MeOH, r.t.; (iv) $HgCl_2$, NaOH/MeOH, r.t.; (v) Au($PPh_3$)Cl, NaOH/MeOH, r.t.

### 2.2. Spectroscopic properties

The IR, NMR ($^1$H, $^{13}$C and $^{31}$P) and MS data of our compounds shown in Section 4 agree with their chemical structures. The solution IR spectra are each characterized by a single sharp $\nu$(C≡C) absorption band at ca. 2098–2144 cm$^{-1}$. The insoluble component of [Hg–T(BP)T]$_\infty$ also exhibits a characteristic solid-state IR $\nu$(C≡C) band, similar to that for the soluble portion. The IR spectrum of each compound shows no band in the range 3200–3300 cm$^{-1}$, characteristic of ≡C–H stretching vibration, thus confirming that the [H–T(BP)T]$_1$ is capped by metal groups via σ bonds. The single $^{31}$P{$^1$H} NMR signals flanked by platinum satellites for [Pt–T(BP)T]$_\infty$ and [Pt–T(BP)T]$_1$ are consistent with a *trans* geometry of the square-planar Pt unit. The $^1J_{P–Pt}$ values in [Pt–T(BP)T]$_\infty$ and [Pt–T(BP)T]$_1$ are typical of those for related *trans*-$PtP_2$ systems [13]. The room-temperature $^{31}$P NMR spectrum of [Au–T(BP)T]$_1$ displays a sharp singlet at $\delta$ 44.04, indicating a symmetrical arrangement of PAuC≡C groups in solution. $^1$H NMR resonances arising from the protons of the organic moieties were observed. The low solubility of [Hg–T(BP)T]$_\infty$ and [Pt–T(BP)T]$_\infty$ led to some difficulties for their complete $^{13}$C NMR characterization but the higher solubility of the model compounds allowed their full $^{13}$C NMR spectra to be interpreted. The formulas of the model complexes [Pt–T(BP)T]$_1$, [Hg–T(BP)T]$_1$ and [Au–T(BP)T]$_1$ were successfully established by the presence of intense molecular ion peaks in their respective positive FAB mass spectra.

### 2.3. Crystal structure analyses

The three-dimensional molecular structures of [Pt–T(BP)T]$_1$, [Au–T(BP)T]$_1$ and [Hg–T(BP)T]$_1$ were analyzed by X-ray crystallography. Perspective views of their structures are shown in Figs. 1–3. Pertinent bond distances and angles are given in Tables 1–3. In each case, the crystal structure consists of discrete binuclear molecules in which two terminal organometallic groups are linked by the biphenyl-spaced bis(acetylide) moiety to afford the expected rod-like skeleton. There are two independent molecules per asymmetric unit in the unit cell of [Pt–T(BP)T]$_1$ and the mean dihedral angle between the two central phenyl planes is ca. 21.5°. For each of [Au–T(BP)T]$_1$ and [Hg–T(BP)T]$_1$, the molecule sits on a crystallographic center of symmetry at the mid-point of the C–C bond between the two planar phenyl rings, resulting in a perfectly coplanar biphenyl unit in the solid-state favorable for π-conjugation. The coordination geometry is square-planar at platinum with the two $PEt_3$ groups *trans* to each other and linear about the gold and mercury centers. The C≡C bond lengths in the ethynyl bridge [1.179(11)–1.193(11) Å for Pt, 1.198(8) Å for Au, and 1.233(16) Å for Hg] are fairly typical of metal–alkynyl σ-bonding. The bond angles for the metal–C≡C units are close to linearity and conform to the rigid-rod nature of these model compounds. By virtue of the fact that [MeHg]$^+$ is isoelectronic and isolobal with the [($PPh_3$)Au]$^+$ fragment, both [Au–T(BP)T]$_1$ and [Hg–T(BP)T]$_1$ have similar structural motifs, reminiscent of other reported examples. The Hg–C (alkyne) bond in [Hg–T(BP)T]$_1$ is slightly longer than the Au–C (alkyne) bond in [Au–T(BP)T]$_1$, but comparable to those in other Hg(II) acetylide compounds [14]. The Hg–$CH_3$ bond (ca. 2.063(12) Å) appears to be shorter than those observed in some methylmercury complexes with thiol ligands [15]. No apparent short intermolecular contacts or π-stacking interactions are observed in our Pt complex. In contrast to many Au(I) compounds, where there frequently exist short Au···Au contacts, aurophilicity is absent in [Au–T(BP)T]$_1$ and the closest intermolecular non-bonded contact is due to an Au(1)···H(26B) interaction (3.097 Å). However, examination of the crystal packing diagram for the Hg(II) counterpart reveals the involvement of ligand-unsupported mercurophilicity in its structure. Remarkably,

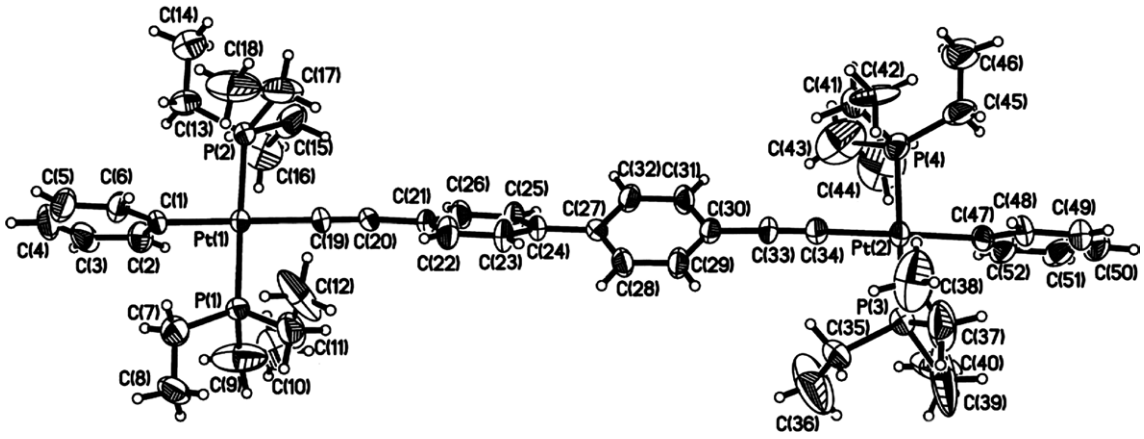


Fig. 1. A perspective drawing of $[Pt–T(BP)T]_1$ with the thermal ellipsoids drawn at the 25% probability level.

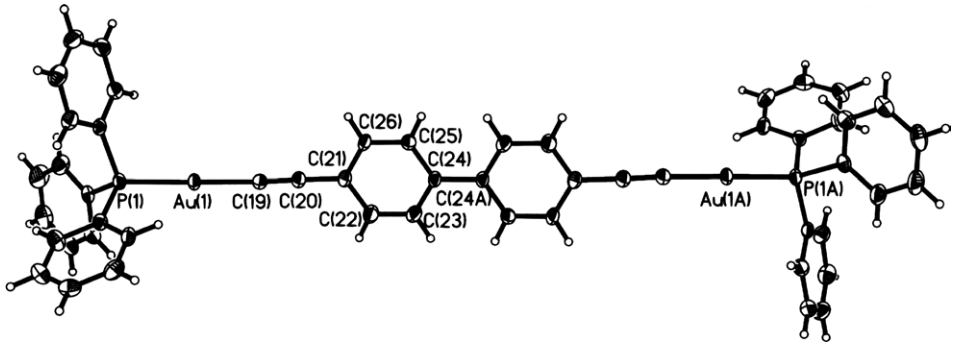


Fig. 2. A perspective drawing of $[Au–T(BP)T]_1$ with the thermal ellipsoids drawn at the 25% probability level.

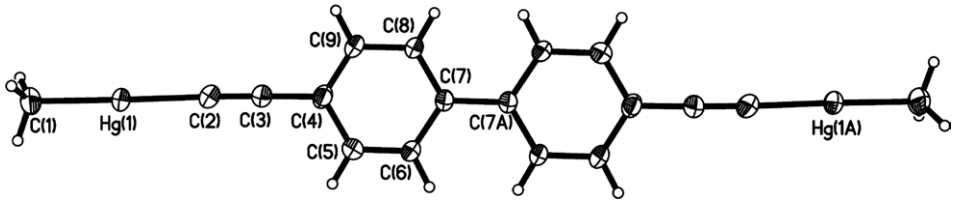


Fig. 3. A perspective drawing of $[Hg–T(BP)T]_1$ with the thermal ellipsoids drawn at the 25% probability level.

there is a strong tendency for the molecules to aggregate together and the whole lattice structure is fully supported and stabilized by extensive non-covalent $d^{10}$–$d^{10}$ Hg···Hg interactive vectors (ca. 3.833, 4.222 and 4.506 Å) that link up the individual molecules in an organized 3D polymeric network (Fig. 4). Although alkynylgold(I) complexes exhibiting Au···Au interactions are numerous [16], literature reports showing Hg···Hg bonding interactions are, to our knowledge, comparatively very limited [17]. While the Hg···Hg contacts here indicate that each of the individual interactions is relatively weak in nature, it is the large number of them that play a supramolecular role and generate a significant driving force for the observation of solid-state aggregation. We conceive that such mercurophilic forces are more than just van der Waals interactions in the present system. In fact, the van der Waals radius of mercury has been the subject of much debate and a value of up to 2.2 Å has been proposed recently [18], which appears to be a better estimate than the value quoted by Bondi in 1964 [19]. So, the observed Hg···Hg separations can be compared to those of 3.71–4.25 Å for mononuclear $[Hg(C{\equiv}CR)_2]$ (R = Ph, $SiMe_3$) [17a], 3.738–4.183 Å for binuclear [MeHgC≡CRC≡CHgMe] (R = 9,9-dioctylfluorenediyl and oligothienyl) [11a] and 4.077 and 4.449 Å computed for molecular $(HgH_2)_n$ clusters ($n = 2$, 3) [17c] and are toward the upper limit of those accepted as representing metallophilic interactions. As shown in Fig. 4, the lattice is characterized by infinite linear chains of Hg atoms between adjacent molecules (e.g., Hg(1B)···Hg(1D)···Hg(1H)···Hg(1L) and Hg(1E)···Hg(1I)···Hg(1M)···Hg(1O)) with the

Table 1
Selected bond lengths (Å) and angles (°) for [Pt–T(BP)T]$_1$

| | Molecule 1 | Molecule 2 | | Molecule 1 | Molecule 2 |
|---|---|---|---|---|---|
| Pt(1)–P(1) | 2.281 (2) | 2.271(3) | Pt(1)–P(2) | 2.274(2) | 2.279(3) |
| Pt(1)–C(1) | 2.081(8) | 2.056(7) | Pt(1)–C(19) | 2.009(8) | 1.998(8) |
| Pt(2)–P(3) | 2.273(3) | 2.270(3) | Pt(2)–P(4) | 2.267(3) | 2.279(3) |
| Pt(2)–C(34) | 2.027(9) | 2.046(9) | Pt(2)–C(47) | 2.069(8) | 2.072(8) |
| C(19)–C(20) | 1.193(11) | 1.192(11) | C(33)–C(34) | 1.179(11) | 1.182(11) |
| P(1)–Pt(1)–P(2) | 176.63(8) | 176.64(10) | P(1)–Pt(1)–C(19) | 89.7(2) | 87.0(3) |
| P(2)–Pt(1)–C(19) | 88.7(2) | 93.2(3) | P(3)–Pt(2)–P(4) | 175.89(10) | 176.50(10) |
| P(3)–Pt(2)–C(34) | 90.8(3) | 88.9(2) | P(4)–Pt(2)–C(34) | 88.7(3) | 87.7(2) |
| Pt(1)–C(19)–C(20) | 179.8(9) | 177.5(9) | C(19)–C(20)–C(21) | 175.0(9) | 174.7(10) |
| Pt(2)–C(34)–C(33) | 175.2(8) | 178.3(9) | C(30)–C(33)–C(34) | 178.6(9) | 177.1(10) |

Table 2
Selected bond lengths (Å) and angles (°) for [Au–T(BP)T]$_1$

| | | | |
|---|---|---|---|
| Au(1)–P(1) | 2.2818(16) | Au(1)–C(19) | 1.996(6) |
| C(19)–C(20) | 1.198(8) | | |
| P(1)–Au(1)–C(19) | 174.68(19) | Au(1)–C(19)–C(20) | 171.3(6) |

Table 3
Selected bond lengths (Å) and angles (°) for [Hg–T(BP)T]$_1$

| | | | |
|---|---|---|---|
| Hg(1)–C(1) | 2.063(12) | Hg(1)–C(2) | 2.031(12) |
| C(2)–C(3) | 1.233(16) | | |
| C(1)–Hg(1)–C(2) | 178.7(4) | C(2)–C(3)–C(4) | 178.7(11) |
| Hg(1)–C(2)–C(3) | 170.8(12) | | |

Hg–Hg–Hg bond angle of 180°. Aggregation of each stack of these molecules also persists throughout the entire crystal lattice in a 3D space via weak Hg···Hg attractive interactions (e.g., Hg(1A)···Hg(1J) 3.833 and Hg(1A)···Hg(1F) 4.222 Å) to form another zigzag chains of Hg centers with the Hg(1A)–Hg(1J)–Hg(1C) and Hg(1C)–Hg(1A)–Hg(1J) angles of 67.8° and 60.2°, respectively. We also locate minor short intermolecular contacts involving the Hg atoms and methyl hydrogen atoms (Hg(1)···H(1B) 3.399 Å) as well as phenyl protons (Hg(1)···HA 3.164 Å) that make only little contribution to the overall molecular packing. This structure is unique in that no apparent weak Hg···$\eta^2$–C≡C interactions are observed which have been shown to be an important driving force for the solid-state aggregation process to take place in alkynyl complexes of Cu(I), Ag(I) and Hg(II) [17b,20].

### 2.4. Thermal analysis

The thermal properties of the polymers were examined by thermal gravimetry (TG) under nitrogen. Analysis of the TG trace (heating rate 20 °C/min) for [Pt–T(BP)T]$_\infty$ and [Hg–T(BP)T]$_\infty$ shows that they exhibit good thermal stability. Decomposition commences at 297 and 330 °C for [Pt–T(BP)T]$_\infty$ and [Hg–T(BP)T]$_\infty$, respectively, and decomposition onset was defined as a mass loss of 2%. While the onset temperature for the former is similar to that found for the prototypical polymer *trans*-[–Pt(PBu$_3$)$_2$C≡C(*p*-C$_6$H$_4$)C≡C–]$_n$ (abbreviated as [Pt–T(P)T]$_\infty$) [21], it is slightly higher than those observed for the related platinum(II) poly-ynes bridged by bipyridyl (274 and 287 °C) [9c] or bithienyl (275 °C) [3b] spacers. The onset of decomposition for [Hg–T(BP)T]$_\infty$ takes place at a higher temperature than those for Hg-containing poly(ethynylenefluorenylene) copolymers (200–280 °C) [10d]. We observe a sharp weight loss of 37% between 295 and 420 °C for [Pt–T(BP)T]$_\infty$, whereas 36% of the weight was lost for [Hg–T(BP)T]$_\infty$ as the temperature rose from 330 to 400 °C. The decomposition step is ascribed to the removal of six butyl groups from [Pt–T(BP)T]$_\infty$ and the loss of one –C≡C-(*p*-C$_6$H$_4$)$_2$– group from [Hg–T(BP)T]$_\infty$.

### 2.5. Electronic absorption and luminescent spectra

The photophysical data of the new compounds measured in both solution and solid state are shown in Table 4. All the metal alkynyls display similar structured absorption bands in the near UV region. The lowest energy transitions are predominantly intraligand in nature consisting of both acetylenic and aromatic $^1(\pi\pi^*)$ character, possibly mixed with some admixture of metal orbitals. The 0–0 absorption peak is assigned as the $S_0 \rightarrow S_1$ transition from the highest occupied molecular orbital (HOMO) to the lowest unoccupied molecular orbital (LUMO), which are mainly delocalized π and π* orbitals [9]. Coordination of each of the metal entities to the organic system results in enhanced $\pi \rightarrow \pi^*$ transitions for the aryleneethynylene moiety. As compared to the band at 289 nm in $CH_2Cl_2$ for [H–T(BP)T]$_1$, we find that the position of the lowest energy absorption band is red-shifted after the inclusion of metal fragment in all the metal alkynyls. This reveals that π-conjugation is preserved through the metal site by mixing of the frontier orbitals of metal and the ligand. In energy terms, the experimentally determined HOMO–LUMO energy gaps ($E_g$) as measured from the onset wavelength in solid film state are also tabulated in Table 4. The transition

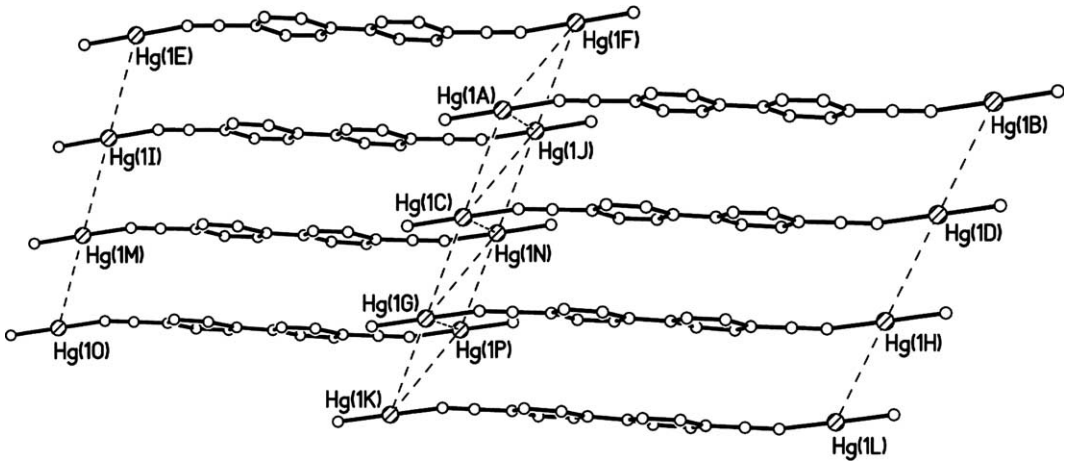


Fig. 4. Crystal packing diagram for $[Hg–T(BP)T]_1$ showing the linear and zigzag chains of Hg atoms aggregated through Hg···Hg intermolecular contacts and all hydrogen atoms are omitted for clarity.

Table 4
Photophysical data for the model complexes and polymers

| | $\lambda_{max}$ (nm)[a] | | $E_g$ (eV)[b] | $\lambda_{em}$ (nm)[c] | |
|---|---|---|---|---|---|
| | $CH_2Cl_2$ | Film | | $CH_2Cl_2$ (290 K)[d] | Frozen $CH_2Cl_2$ (77 K)[e] |
| $[Pt–T(BP)T]_1$ | 305 (3.7) | 352 | 3.17 | 391 | 383* |
| | 349 (11.4) | | | 408* (2.2, 2.0) | 407* |
| | | | | | 542 (0.34) |
| | | | | | 582* |
| $[Pt–T(BP)T]_\infty$ | 304 | 362 | 3.10 | 369* | 418* |
| | 372 | 374 | | 409 (6.0, 2.4) | 549 (0.12) |
| | | | | 556* | 592* |
| $[Hg–T(BP)T]_1$ | 309 (11.7) | 310 | 3.31 | 367 | 395* |
| | | | | 382* (6.0, 2.2) | 420* |
| | | | | | 464 |
| | | | | | 526 (6.7)[f] |
| | | | | | 543* |
| $[Hg–T(BP)T]_\infty$ | 310 | 308 | 3.27 | 371 (3.0, 2.2) | 405br |
| | | | | | 523 (3.9)[f] |
| | | | | | 551 |
| $[Au–T(BP)T]_1$ | 326 (53.7) | 342 | 3.24 | 365* | 376* |
| | | | | 383 (1.6, 1.0) | 396* |
| | | | | | 529 (0.10) |
| | | | | | 568* |
| $[H–T(BP)T]_1$ | 289 (3.8) | 270 | 3.50 | | |

[a] Extinction coefficients ($10^4$ $M^{-1}$ $cm^{-1}$) are shown in parentheses.
[b] Estimated from the onset wavelength of the solid-state optical absorption.
[c] Asterisks indicate that emission peaks appear as shoulders or weak bands.
[d] Fluorescence quantum yields (%) and lifetimes (ns) shown in parentheses ($\Phi_F$, $\tau_F$) are measured in $CH_2Cl_2$ relative to anthracene.
[e] Phosphorescence lifetimes $\tau_P$ (μs) at 20 K for the peak maxima are shown in parentheses.
[f] $\tau_P$ (μs) was measured at 77 K; br = broad.

energies of the long-chain polymer $[Pt–T(BP)T]_\infty$ are lowered with respect to those of $[Pt–T(BP)T]_1$, suggesting a well-extended singlet excited state in the Pt(II) polymer. According to the type of the metal groups, the optical energy gaps of the poly-ynes follow the experimental order $[Hg–T(BP)]T]_\infty > [Pt–T(BP)T]_\infty$ and those of the model compounds $[Hg–T(BP)T]_1 > [Au–T(BP)T]_1 > [Pt–T(BP)T]_1$.

At 290 K, all of the complexes in $CH_2Cl_2$ solution emit purple-blue $^1(\pi\pi^*)$ fluorescence ($S_1 \rightarrow S_0$) peak near 400 nm that is characterized by the small Stokes shift between the bands in the absorption and the emission spectra. At 77 K, the principal emission peak occurs at ca. 549 and 523 nm for $[Pt–T(BP)T]_\infty$ and $[Hg–T(BP)T]_\infty$, and at ca. 542, 529 and 526 nm for $[Pt–T(BP)T]_1$, $[Au–T(BP)T]_1$ and $[Hg–T(BP)T]_1$,

respectively. The large Stokes shifts of these lower-lying emission peaks from the dipole-allowed absorptions (1.08–1.66 eV, see Figs. 5–9), plus the long emission lifetimes ($\tau_P$) in the microsecond regime are indicative of their triplet parentage, and they are thus assigned to the $^3(\pi\pi^*)$ excited states of the 4,4′-diethynylbiphenyl core (i.e., $T_1 \rightarrow S_0$ emission). Such assignment can be further supported by the observed temperature dependence of the emission data for $[Pt–T(BP)T]_\infty$ (see Fig. 10), in accordance with earlier work on platinum(II) poly-ynes [9]. From 290 to 20 K, the singlet emission peak intensity increases only by a factor of 3.8 but the intensity of the lower-lying triplet emission increases by a factor of 61.2 which is accompanied by a well-resolved vibronic structure, and such an increase in intensity indicates a long-lived triplet excited state that is more sensitive to thermally activated non-radiative decay mechanisms. For $[Hg–T(BP)T]_1$, an emission band also appears at 464 nm presumably due to the formation of solid-state aggregates in frozen $CH_2Cl_2$ [10d,22] and this corroborates well with the results from X-ray structural analysis (vide supra). The observation of a broad band centered at ~405 nm (spanning up to ~500 nm) in the photoluminescence spectrum of $[Hg–T(BP)T]_\infty$ is also a manifestation of the solid-state aggregation effect.

Based on the absorption and photoluminescence data, we can obtain experimental values of the lower-lying excitations (Table 5) and construct an energy scheme as shown in Fig. 11 for the polymers and the model complexes that allows thorough investigation of the spatial extent of the singlet and triplet excitons. The energy values are absolute values with respect to the $S_0$ ground state. Values of $\Delta E(S_0 - T_1)$ (energy gap between $S_0$ and $T_1$) were compiled to be 2.26–2.36 eV for all the metal di-ynes and poly-ynes. The measured $\Delta E(S_1 - T_1)$ values are 0.76, 0.71, 0.76, 0.70 and 0.79 eV for $[Pt–T(BP)T]_1$, $[Pt–T(BP)T]_\infty$, $[Hg–T(BP)T]_1$, $[Hg–T(BP)T]_\infty$

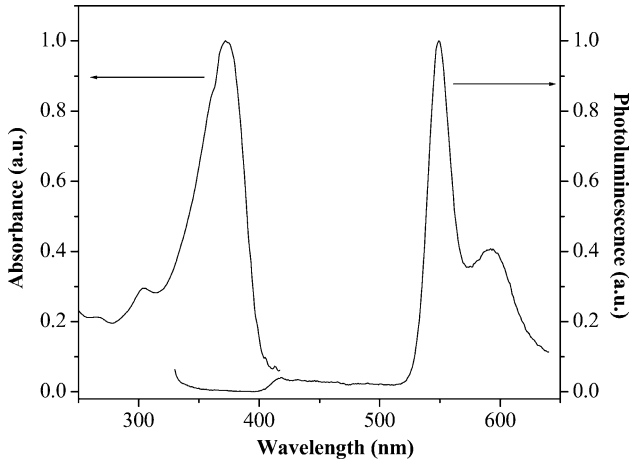


Fig. 6. Room temperature optical absorption spectrum and photoluminescence spectrum (77 K) of $[Pt–T(BP)T]_\infty$ in $CH_2Cl_2$.

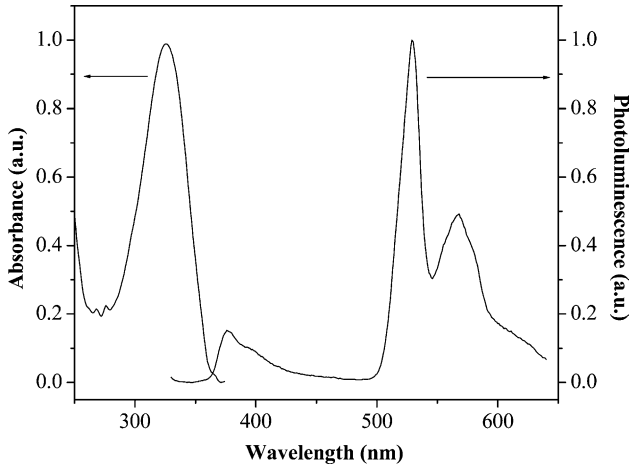


Fig. 7. Room temperature optical absorption spectrum and photoluminescence spectrum (77 K) of $[Au–T(BP)T]_1$ in $CH_2Cl_2$.

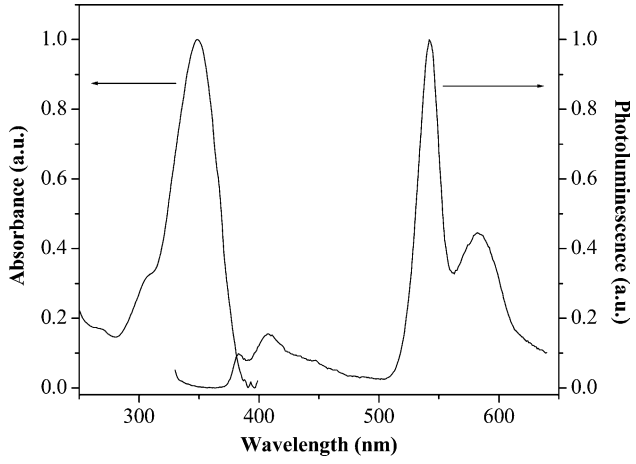


Fig. 5. Room temperature optical absorption spectrum and photoluminescence spectrum (77 K) of $[Pt–T(BP)T]_1$ in $CH_2Cl_2$.

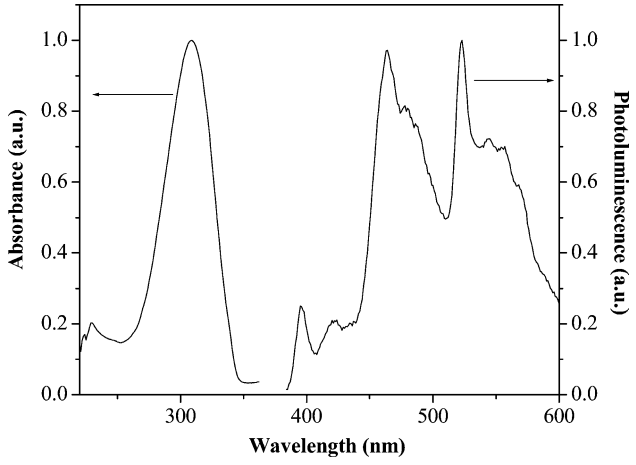


Fig. 8. Room temperature optical absorption spectrum and photoluminescence spectrum (77 K) of $[Hg–T(BP)T]_1$ in $CH_2Cl_2$.

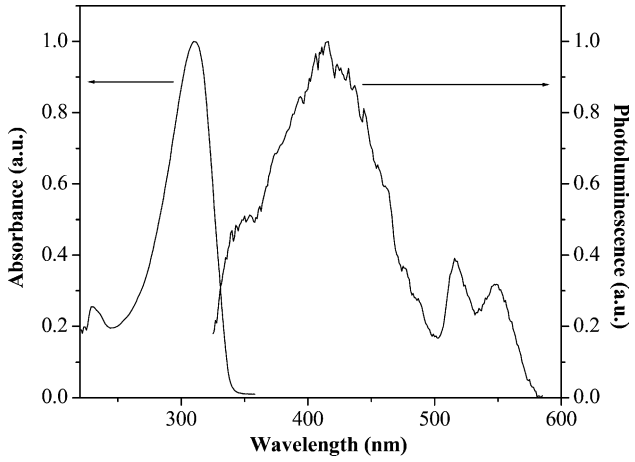


Fig. 9. Room temperature optical absorption spectrum and photoluminescence spectrum (77 K) of $[Hg–T(BP)T]_\infty$ in $CH_2Cl_2$.

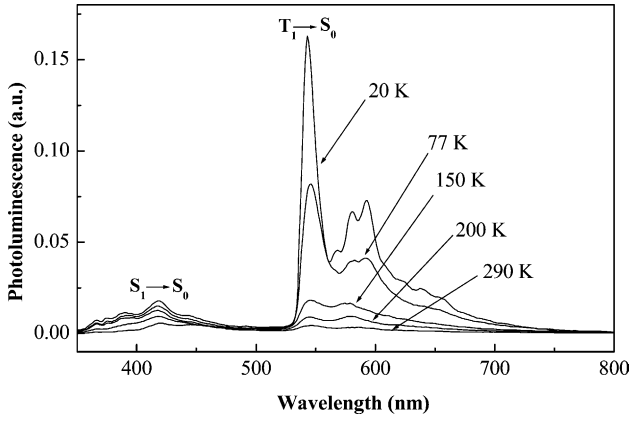


Fig. 10. Temperature dependence of the photoluminescence of $[Pt–T(BP)T]_\infty$.

and $[Au–T(BP)T]_1$, respectively, and they correspond well with the $S_1 - T_1$ energy gap of $0.7 \pm 0.1$ eV for similar π-conjugated Pt(II), Au(I) and Hg(II) poly-ynes [9a,10a,10d], and are close to the gaps estimated for a series of related organic conjugated polymers [23]. We attribute such a constant $\Delta E(S_1 - T_1)$ value to the exchange energy and possibly some additional constant contribution due to the admixture of the metal orbitals [9d]. From the $S_1$ energy levels obtained by absorption studies, it is clear that the $S_1$ states are notably lower for the $d^8$ Pt(II) species than those for the $d^{10}$ Au(I) and Hg(II) congeners. The order of π-delocalization through the metal chromophore is Pt(II) > Au(I) > Hg(II). For the Pt(II) and Hg(II) systems, the lowest $T_1$ state remains strongly localized, as can be inferred from the small energy difference between triplet emissions in the metal di-ynes and in the poly-ynes. Previous calculations carried out for $[Pt–T(P)T]_\infty$ also indicated the triplet to be confined onto the phenylene ring [24]. Substitution of the metal groups does not seem to alter this strong confinement. We observe that the energy levels for the Pt di-yne and poly-yne are red-shifted relative to $[Pt–T(P)T]_1$ and $[Pt–T(P)T]_\infty$ (P = *p*-phenylene) in which the presence of two phenyl rings in the former cases was shown to increase the π-conjugation length and can shift the phosphorescence to the red by 0.10 and 0.12 eV, respectively. The energy of the $T_1 \rightarrow S_0$ transition also varies with the organometallic groups. Apparently, the $T_1$ levels for the Au(I) and Hg(II) compounds are slightly higher than those for the corresponding Pt(II) congeners in the present system. We note that the order of $S_1 \rightarrow T_1$ crossover efficiency is $[Au–T(BP)T]_1 > [Pt–T(BP)T]_1$, since the energy of the $T_1$ state is higher for the former, resulting in a faster phosphorescence radiative decay rate. This also agrees with the results obtained from the peak height ratio from triplet emission to singlet emission at 77 K, $\Delta E(T_1 \rightarrow S_0,\ S_1 \rightarrow S_0)$ (Table 5), which has been adopted previously as a good parameter to evaluate the relative ISC efficiency [9e,9f,9i]. An order of ISC efficiency $[Pt–T(BP)T]_\infty > [Pt–T(BP)T]_1$ is observed, similar to the Pt system with a single phenyl ring. Based on the work by others that the ISC efficiency is close to unity for third row transition metal chromophores [25], the radiative ($k_r$) and non-radiative ($k_{nr}$) decay rates are related to the measured lifetime of triplet emission ($\tau_P$) and the phosphorescence quantum yield ($\Phi_P$) by the following expressions:

$$k_{nr} = (1 - \Phi_P)/\tau_P,$$

$$k_r = \Phi_P/\tau_P.$$

Table 5
Experimental values of various transition energies among the $S_0$, $S_1$ and $T_1$ levels and intersystem crossing efficiencies of platinum(II), gold(I) and mercury(II) di-ynes and poly-ynes containing biphenyl groups

| Energy (eV) | $[Pt–T(BP)T]_1$ | $[Pt–T(BP)T]_\infty$ | $[Hg–T(BP)T]_1$ | $[Hg–T(BP)T]_\infty$ | $[Au–T(BP)T]_1$ |
|---|---|---|---|---|---|
| $S_0 \rightarrow S_1$ | 3.55 | 3.33 | 4.01 | 4.00 | 3.80 |
| $S_1 \rightarrow S_0$ | 3.05 | 2.97 | 3.12 | 3.06 | 3.13 |
| $T_1 \rightarrow S_0$ | 2.29 | 2.26 | 2.36 | 2.36 | 2.34 |
| $S_1 \rightarrow T_1$ | 0.76 | 0.71 | 0.76 | 0.70 | 0.79 |
| $\Delta E(T_1 \rightarrow S_0, S_1 \rightarrow S_0)$[a] | 6.0 | 18.9 | [b] | [b] | 9.1 |

[a] Ratio of the intensities of triplet emission to singlet emission at 77 K.
[b] Cannot be accurately determined due to the presence of broad aggregate emission band.

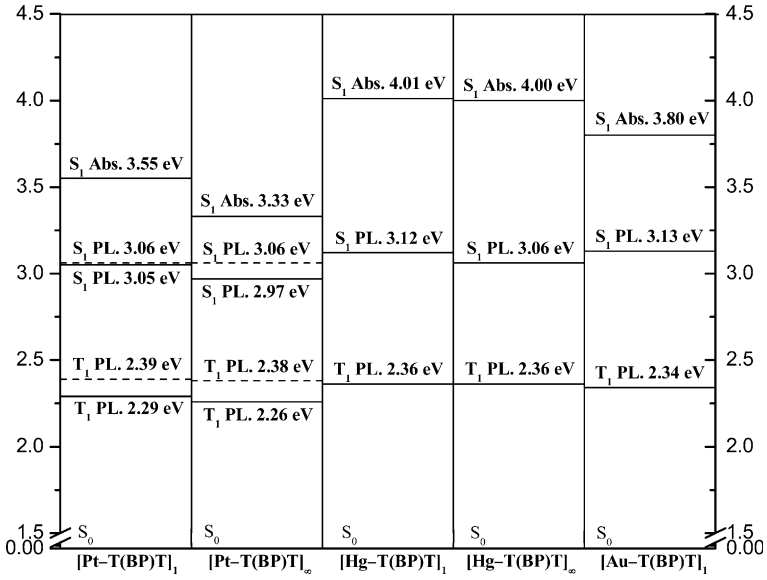


Fig. 11. Electronic energy level diagram of biphenyl-linked metal alkynyls determined from absorption and emission data. Dashed lines represent the levels for $[Pt–T(P)T]_l$ and $[Pt–T(P)T]_\infty$ and the data were taken from Ref. [9e]. The $S_0$ levels are arbitrarily shown to be of equal energy.

Table 6
The measured phosphorescence quantum yields, lifetimes, and radiative and non-radiative decay rates of $[Pt–T(BP)T]_l$, $[Pt–T(BP)T]_\infty$ and $[Au–T(BP)T]_l$ at 20 K

| | $\Phi_P$ (%) | $\tau_P$ (μs) | $(k_{nr})_P$ ($s^{-1}$) | $(k_r)_P$ ($s^{-1}$) |
|---|---|---|---|---|
| $[Pt–T(BP)T]_l$ | 26.4 | 0.34 | $2.2\times10^6$ | $7.8\times10^5$ |
| $[Pt–T(BP)T]_\infty$ | 23.9 | 0.12 | $6.6\times10^6$ | $2.1\times10^6$ |
| $[Au–T(BP)T]_l$ | 18.6 | 0.10 | $7.8\times10^6$ | $1.8\times10^6$ |

The measured $\Phi_P$ and $\tau_P$ values for $[Pt–T(BP)T]_l$ are 0.26 and 0.34 μs at 20 K, respectively, and those for $[Au–T(BP)T]_l$ are 0.19 and 0.10 μs. The values calculated for $k_{nr}$ and $k_r$ at 20 K for both Pt and Au di-ynes are given in Table 6. For phosphorescence in aromatic hydrocarbon molecules, $k_r$ lies typically between 0.1 and 1 $s^{-1}$ [26]. So, the heavy-atom effect of Pt and Au can speed up the radiative decay rate for the triplet emission by 5–6 orders of magnitude and the phosphorescence decay rate for $[Au–T(BP)T]_l$ ($k_r \sim 1.8\times10^6$ $s^{-1}$) is about twice that of $[Pt–T(BP)T]_l$ ($k_r \sim 7.8\times10^5$ $s^{-1}$). However, for the sake of accuracy, no attempts were made to compare the results with $[Hg–T(BP)T]_l$ because of the aggregate emission band that is present which would provide another possible radiative decay pathway.

## 3. Concluding remarks

This report demonstrated that 4,4′-diethynylbiphenyl is a useful precursor to afford a new series of luminescent bimetallic and organometallic poly-yne materials of group 10–12 transition metals. On the structural aspect, depending on the steric properties of the end groups anchored on the alkynyl unit, we were able to build up polymeric mercury(II) acetylide system in the solid state aggregated through Hg···Hg secondary interactions. All the compounds were analytically and spectroscopically characterized to possess a well-defined size and structure. The materials are solution-processable and thermally stable. All the three transition metals (viz., Pt, Au, and Hg) can exert heavy-atom effects in the enhancement of ISC rate and a discussion was made on the relation between the $T_1$ energy state and the $k_r$ value for the triplet emission. It is envisioned that a structure–property–function relationship can be established and valuable insight into the photophysical nature of $(–C{\equiv}C–Ar–C{\equiv}C–)_n$ conjugated materials can be subsequently derived. Future work in this direction should elucidate a direct evaluation of the role of a metal center on the properties of conjugated compounds and such an investigation is desirable for optoelectronic applications that utilize the $T_1$ state for light emission through light-harvesting techniques.

## 4. Experimental

### 4.1. General procedures

All reactions were carried out under a nitrogen atmosphere using standard Schlenk techniques, but no special precautions were taken to exclude oxygen during work-up. Solvents were predried and distilled from appropriate drying agents. All reagents and chemicals, unless otherwise stated, were purchased from commercial sources and used without further purification. Preparative TLC was performed on 0.7 mm silica plates (Merck

Kieselgel 60 $GF_{254}$) prepared in our laboratory. The compounds $[H–T(BP)T]_1$ [27], *trans*-$[PtCl(Ph)(PEt_3)_2]$ [28] and *trans*-$[PtCl_2(PBu_3)_2]$ [29] were prepared by literature methods. Infrared spectra were recorded as $CH_2Cl_2$ solutions or KBr pellets using a Perkin–Elmer Paragon 1000 PC or Nicolet Magna 550 Series II FTIR spectrometer. NMR spectra were measured in $CDCl_3$ on a Jeol EX270 or a Varian Inova 400 MHz FT NMR spectrometer, with $^1H$ and $^{13}C$ NMR chemical shifts quoted relative to TMS and $^{31}P$ chemical shifts relative to an 85% $H_3PO_4$ external standard. Fast atom bombardment (FAB) mass spectra were recorded on a Finnigan MAT SSQ710 mass spectrometer. Electronic absorption spectra were obtained with a HP 8453 UV–vis spectrometer. For solid-state emission spectral measurements, the 325 nm line of a He–Cd laser was used as an excitation source. The luminescence spectra were analyzed by a 0.25 m focal length double monochromator with a Peltier cooled photomultiplier tube and processed with a lock-in-amplifier. For the low temperature experiments, samples were mounted in a closed-cycle cryostat (Oxford CC1104) in which the temperature can be adjusted from 10 to 330 K. The solution emission spectra at 290 and 77 K were measured on a PTI Fluorescence Master Series QM1 spectrophotometer. The fluorescence quantum yields ($\Phi_F$) were determined in $CH_2Cl_2$ at 290 K against the anthracene standard ($\Phi_F = 0.27$). Phosphorescence quantum yields $\Phi_P$ were measured in solid thin films at 20 K relative to the prototypical polymer *trans*-$[–Pt(PBu_3)_2C{\equiv}C(p\text{-}C_6H_4)C{\equiv}C–]_n$ ($\Phi_P = 0.30$ at 20 K) [9a]. The molecular weights of the polymers were determined by GPC (HP 1050 series HPLC with visible wavelength and fluorescent detectors) using polystyrene standards and thermal analyses were performed with a Perkin–Elmer TGA6 thermal analyzer.

### 4.2. Preparations of complexes

#### 4.2.1. Synthesis of $[Pt–T(BP)T]_\infty$

A mixture of 4,4′-diethynylbiphenyl, $[H–T(BP)T]_1$, (11.0 mg, 0.054 mmol) and *trans*-$[PtCl_2(PBu_3)_2]$ (36.5 mg, 0.054 mmol) in a 1:1 molar ratio in $^iPr_2NH/CH_2Cl_2$ (10 $cm^3$, 1:1, v/v) was allowed to react in the presence of CuI (3.0 mg). The solution was stirred at r.t. for 15 h, after which all volatile components were removed under reduced pressure. The residue was taken up in $CH_2Cl_2$ and filtered through a silica gel column using the same solvent as the eluent to give a yellow solution. Upon removal of solvent, the product was then reprecipitated twice from a $CH_2Cl_2$/MeOH mixture followed by washing with MeOH to afford a light yellow powder in 65% yield (28.3 mg). IR ($CH_2Cl_2$): $\nu$(C≡C) 2101 $cm^{-1}$. $^1H$ NMR ($CDCl_3$): $\delta$ 7.45 (d, $J = 6.8$ Hz, 4H, Ar), 7.29 (d, $J = 6.8$ Hz, 4H, Ar), 2.18 (m, 12H, $PCH_2$), 1.61 (m, 12H, $PCH_2CH_2$), 1.46 (m, 12H, $P(CH_2)_2CH_2CH_3$) and 0.94 (m, 18H, $CH_3$) ppm. $^{31}P\{^1H\}$ NMR ($CDCl_3$): $\delta$ 4.12 ($^1J_{Pt–P} = 2356$ Hz) ppm. Anal. Found: C, 59.82; H, 7.68. Calc. for $(C_{40}H_{62}PtP_2)_n$: C, 60.06; H, 7.81%. GPC (THF as eluent): $M_w = 14770$, $M_n = 13060$, polydispersity = 1.13.

#### 4.2.2. Synthesis of $[Pt–T(BP)T]_1$

A solution of $[H–T(BP)T]_1$ (9.1 mg, 0.045 mmol) and two molar equivalents of *trans*-$[PtCl(Ph)(PEt_3)_2]$ (48.9 mg, 0.090 mmol) in $^iPr_2NH/CH_2Cl_2$ (10 $cm^3$, 1:1, v/v) was charged into a 50 mL Schlenk flask and a small amount of CuI (3.0 mg) was then added. The resulting mixture was stirred at r.t. over a period of 15 h, after which all the volatile components were evaporated to dryness. The residue was redissolved in $CH_2Cl_2$ and the solution was purified on preparative TLC plates eluting with hexane/$CH_2Cl_2$ (3:2, v/v, $R_f = 0.55$) to give the title complex as an off-white crystalline solid with an isolated yield of 67% (36.7 mg). IR ($CH_2Cl_2$): $\nu$(C≡C) 2098 $cm^{-1}$. $^1H$ NMR ($CDCl_3$): $\delta$ 7.37 (d, $J = 7.8$ Hz, 4H, Ar), 7.28–7.18 (m, 8H, Ar + $H_{ortho}$ of Ph–Pt), 6.89 (t, $J = 7.6$ Hz, 4H, $H_{meta}$ of Ph–Pt), 6.74 (t, $J = 7.6$ Hz, 2H, $H_{para}$ of Ph–Pt), 1.71 (m, 24 H, $CH_2CH_3$) and 1.03 (m, 36H, $CH_2CH_3$) ppm. $^{13}C$ NMR ($CDCl_3$): $\delta$ 156.28, 139.05, 137.09, 131.02, 127.94, 127.16, 126.08, 121.09 (Ar), 114.18, 110.06 (C≡C), 15.19 and 8.14 (Et) ppm. $^{31}P\{^1H\}$ NMR ($CDCl_3$): $\delta$ 11.67 ($^1J_{Pt–P} = 2628$ Hz) ppm. FAB-MS: *m/z* 1217 [$M^+$]. Anal. Found: C, 51.02; H, 6.50. Calc. for $C_{52}H_{78}Pt_2P_4$: C, 51.31; H, 6.46%.

#### 4.2.3. Synthesis of $[Hg–T(BP)T]_\infty$

A solution of $HgCl_2$ (25.6 mg, 0.094 mmol) in MeOH (10 $cm^3$) was mixed with $[H–T(BP)T]_1$ (19.1 mg, 0.094 mmol) in MeOH (10 $cm^3$). To this mixture, 1.9 $cm^3$ of 0.20 M basic MeOH (0.38 mmol, prepared by dissolving 0.40 g of NaOH in 50 $cm^3$ of MeOH) was added. Within several minutes, an off-white solid precipitated from the homogeneous solution. The reaction was complete after stirring for 12 h and the solid was collected by filtration, washed with MeOH ($2 \times 20$ $cm^3$), and air-dried to furnish the polymer in 80% yield (30.3 mg). IR ($CH_2Cl_2$): $\nu$(C≡C) 2138 $cm^{-1}$. $^1H$ NMR ($CDCl_3$): $\delta$ 7.56 (t, $J = 8.6$ Hz, 4H, Ar) and 6.93 (d, $J = 8.6$ Hz, 4H, Ar) ppm. Anal. Found: C, 47.65; H, 1.88. Calc. for $(C_{16}H_8Hg)_n$: C, 47.94; H, 2.01%. GPC (THF as eluent): $M_w = 2390$, $M_n = 2200$, polydispersity = 1.09.

#### 4.2.4. Synthesis of $[Hg–T(BP)T]_1$

The organic di-yne $[H–T(BP)T]_1$ (13.0 mg, 0.064 mmol) in MeOH (10 $cm^3$) was first combined with MeHgCl (37.1 mg, 0.15 mmol) in MeOH (10 $cm^3$). 0.20 M basic MeOH (1.3 mL, 0.26 mmol) was subsequently added to produce a pale yellow suspension.

The solvent was then decanted and the light yellow solid (32.5 mg, 80%) was washed with MeOH ($2 \times 10\ cm^3$) and air-dried. IR ($CH_2Cl_2$): $\nu$(C≡C) 2138 $cm^{-1}$. $^1H$ NMR ($CDCl_3$): $\delta$ 7.52 (m, 8H, Ar) and 0.71 (s, $^2J$(Hg–H) = 147 Hz, 6H, $CH_3$) ppm. $^{13}C$ NMR ($CDCl_3$): $\delta$ 144.18, 140.06, 132.82, 127.03 (Ar), 105.25 (C≡C) and 7.35 ($CH_3$) ppm. FAB-MS: *m/z* 631 [$M^+$]. Anal. Found: C, 34.02; H, 2.10. Calc. for $C_{18}H_{14}Hg_2$: C, 34.24; H, 2.23%.

#### 4.2.5. Synthesis of [Au–T(BP)T]$_1$

To the solution of [H–T(BP)T]$_1$ (8.2 mg, 0.041 mmol) in MeOH (10 $cm^3$) was added two molar equivalents of Au(PPh$_3$)Cl (43.1 mg, 0.087 mmol), followed by a solution of NaOMe/MeOH (0.20 M, 0.16 mmol, 0.8 $cm^3$). The mixture was stirred at r.t. overnight and the pale yellow powdery solid was then collected by decantation which was washed with MeOH ($2 \times 10\ cm^3$) and air-dried to give 44.4 mg (97%) of the pure product. IR ($CH_2Cl_2$): $\nu$(C≡C) 2144 $cm^{-1}$. $^1H$ NMR ($CDCl_3$): $\delta$ 7.50 (m, 38H, Ar) ppm. $^{13}C$ NMR ($CDCl_3$): $\delta$ 139.12, 134.63, 134.49, 132.99, 131.80, 130.24, 129.45, 129.33, 126.64, 123.98 (Ar), 104.52 (C≡C) ppm. $^{31}P\{^1H\}$ NMR ($CDCl_3$): $\delta$ 44.04 ppm. FAB-MS: *m/z* 1119 [$M^+$]. Anal. Found: C, 55.58; H, 3.35. Calc. for $C_{52}H_{38}Au_2P_2$: C, 55.83; H, 3.42%.

## 5. Crystallography

Single crystals of [Pt–T(BP)T]$_1$, [Au–T(BP)T]$_1$ and [Hg–T(BP)T]$_1$ suitable for X-ray crystallographic analyses were grown by slow evaporation of their respective solutions in $CH_2Cl_2$–hexane at r.t. The crystals were chosen and mounted on a glass fiber using epoxy resin. Crystal data, data collection parameters and results of the analyses are listed in Table 7. The diffraction experiments were carried out at r.t. on a Bruker Axs SMART 1000 CCD area-detector diffractometer using graphite-monochromated Mo Kα radiation ($\lambda = 0.71073$ Å). The raw intensity data frames were integrated with the SAINT+ program using a narrow-frame integration algorithm [30]. Corrections for Lorentz and polarization effects were also applied by SAINT. For each analysis, an empirical absorption correction based on the multiple measurement of equivalent reflections was applied by using the program SADABS [31]. The structures were solved by direct methods and expanded by difference Fourier syntheses using the software SHELTXL [32]. Structure refinements were made on $F^2$ by the full-matrix least-squares technique. In each case, all the non-hydrogen atoms were refined with anisotropic displacement parameters. The hydrogen atoms were placed in their ideal positions but not refined.

Table 7
Summary of crystal structure data for [Pt–T(BP)T]$_1$, [Au–T(BP)T]$_1$ and [Hg–T(BP)T]$_1$

| | [Pt–T(BP)T]$_1$ | [Au–T(BP)T]$_1$ | [Hg–T(BP)T]$_1$ |
|---|---|---|---|
| Empirical formula | $C_{52}H_{78}P_4Pt_2$ | $C_{52}H_{38}Au_2P_2$ | $C_{18}H_{14}Hg_2$ |
| Molecular weight | 1217.20 | 1118.70 | 631.47 |
| Crystal size (mm) | $0.30 \times 0.22 \times 0.20$ | $0.20 \times 0.10 \times 0.08$ | $0.22 \times 0.16 \times 0.10$ |
| Crystal system | Triclinic | Triclinic | Triclinic |
| Space group | $P\bar{1}$ | $P\bar{1}$ | $P\bar{1}$ |
| $a$ (Å) | 9.476(6) | 6.7962(6) | 4.5058(6) |
| $b$ (Å) | 17.300(11) | 10.6022(9) | 8.8672(11) |
| $c$ (Å) | 34.13(2) | 14.8133(13) | 10.0227(12) |
| $\alpha$ (°) | 76.951(12) | 100.380(2) | 96.419(2) |
| $\beta$ (°) | 86.479(12) | 102.077(2) | 96.422(2) |
| $\gamma$ (°) | 84.269(12) | 90.032(2) | 97.915(2) |
| $U$ (Å$^3$) | 5419(6) | 1025.85(15) | 390.84(9) |
| $D_{calc}$ (g $cm^{-3}$) | 1.492 | 1.811 | 2.683 |
| $Z$ | 4 | 1 | 1 |
| $\mu$(Mo Kα) ($mm^{-1}$) | 5.306 | 7.257 | 19.603 |
| $F$(000) | 2424 | 538 | 282 |
| $\theta$ angle (°) | 0.61–23.32 | 1.95–24.99 | 2.06–25.00 |
| Reflections collected | 45235 | 5132 | 1657 |
| Unique reflections | 15605 | 3548 | 1200 |
| $R_{int}$ | 0.0638 | 0.0259 | 0.0278 |
| Observed reflections [$I > 2\sigma(I)$] | 10750 | 2951 | 1118 |
| No. of parameters | 1045 | 253 | 92 |
| $R_1$, $wR_2$ [$I > 2\sigma(I)$] | 0.0600, 0.1237 | 0.0329, 0.0676 | 0.0371, 0.0984 |
| $R_1$, $wR_2$ (all data) | 0.0919, 0.1356 | 0.0469, 0.0731 | 0.0390, 0.1001 |
| Goodness-of-fit on $F^2$ | 1.108 | 1.024 | 1.047 |
| Residual extrema in final difference map (e Å$^{-3}$) | 1.278 to −1.416 | 0.716 to −0.654 | 1.731 to −1.053 |

## 6. Supplementary material

Crystallographic data (comprising hydrogen atom coordinates, thermal parameters and full tables of bond lengths and angles) for the structural analysis have been deposited with the Cambridge Crystallographic Centre (Deposition Nos. 261310–261312). Copies of this information may be obtained free of charge from The Director, CCDC, 12 Union Road, Cambridge, CB2 1EZ, UK (Fax: + 44 1223 336 033; e-mail: deposit@ccdc.cam.ac.uk or www: http://www.ccdc.cam.ac.uk).

## Acknowledgments

Financial support from a CERG Grant from the Hong Kong Research Grants Council of the Hong Kong SAR, PR China (Project No. HKBU2048/01P) is gratefully acknowledged. We also thank Dr. K.-W. Cheah for the access of the facilities for variable temperature photoluminescence measurements.

## References

[1] (a) J.L. Brédas, R.R. Chance (Eds.), Conjugated Polymeric Materials: Opportunities in Electronics, Optoelectronics and Molecular Electronics, Kluwer Academic Publishers, Dordrecht, 1990;
(b) Y. Shirota, J. Mater. Chem. 10 (2000) 1;
(c) U. Mitschke, P. Bäuerle, J. Mater. Chem. 10 (2000) 1471;
(d) C.D. Entwistle, T.B. Marder, Chem. Mater. 16 (2004) 4574;
(e) C.H. Chen, J. Shi, Coord. Chem. Rev. 171 (1998) 161;
(f) B.J. Coe, N.R.M. Curati, Comments Inorg. Chem. 25 (2004) 147;
(g) T.A. Skotheim, J.R. Reynolds, R.L. Elsenbaumer (Eds.), Handbook of Conducting Polymers, second ed., Marcel Dekker, New York, 1998.

[2] (a) J.H. Burroughes, D.D.C. Bradley, A.R. Brown, R.N. Marks, K. Mackay, R.H. Friend, P.L. Burn, A.B. Holmes, Nature (London) 347 (1990) 539;
(b) A. Kraft, A.C. Grimsdale, A.B. Holmes, Angew. Chem. Int. Ed. 37 (1998) 402;
(c) R.H. Friend, R.W. Gymer, A.B. Holmes, J.H. Burroughes, R.N. Marks, C. Taliani, D.D.C. Bradley, D.A. Dos Santos, J.L. Brédas, M. Lögdlund, W.R. Salaneck, Nature (London) 397 (1999) 121.

[3] (a) J.M. Halls, C.A. Walsh, N.C. Greenham, E.A. Marseglia, R.H. Friend, S.C. Moratti, A.B. Holmes, Nature (London) 376 (1995) 498;
(b) G. Yu, J. Gao, J.C. Hummelen, F. Wudl, A.J. Heeger, Science 270 (1995) 1789;
(c) N. Chawdhury, A. Köhler, R.H. Friend, W.-Y. Wong, J. Lewis, M. Younus, P.R. Raithby, T.C. Corcoran, M.R.A. Al-Mandhary, M.S. Khan, J. Chem. Phys. 110 (1999) 4963;
(d) A. Köhler, H.F. Wittmann, R.H. Friend, M.S. Khan, J. Lewis, Synth. Met. 67 (1994) 245;
(e) W.K. Chan, C.S. Hui, K.Y.K. Man, K.W. Cheng, H.L. Wong, N. Zhu, A.B. Djurišć, Coord. Chem. Rev. (in press);
(f) N. Chawdhury, M. Younus, P.R. Raithby, J. Lewis, R.H. Friend, Opt. Mater. 9 (1998) 498;
(g) M. Younus, A. Köhler, S. Cron, N. Chawdhury, M.R.A. Al-Mandhary, M.S. Khan, J. Lewis, N.J. Long, R.H. Friend, P.R. Raithby, Angew. Chem. Int. Ed. 37 (1998) 3036.

[4] (a) Q.-Z. Yang, L.-Z. Wu, H. Zhang, B. Chen, Z.-X. Wu, L.-P. Zhang, C.-H. Tung, Inorg. Chem. 43 (2004) 5195;
(b) P.K.M. Siu, S.W. Lai, W. Lu, N. Zhu, C.M. Che, Eur. J. Inorg. Chem. (2003) 2749;
(c) I.-B. Kim, B. Erdogan, J.N. Wilson, U.H.F. Bunz, Chem. Eur. J. 10 (2004) 6247.

[5] (a) F. Garnier, R. Hajlaoui, A. Yasser, P. Svwastra, Science 265 (1994) 1684;
(b) H. Sirringhaus, N. Tissler, R.H. Friend, Science 280 (1998) 1741.

[6] (a) N.J. Long, Angew. Chem., Int. Ed. Engl. 34 (1995) 21;
(b) S.R. Marder, in: D.W. Bruce, D. O'Hare (Eds.), Inorganic Materials, Wiley, Chichester, 1996, p. 121;
(c) S. Barlow, D. O'Hare, Chem. Rev. 97 (1997) 637;
(d) I.R. Whittal, A.M. McDonagh, M.G. Humphrey, Adv. Organomet. Chem. 42 (1998) 291.

[7] (a) J.S. Wilson, A.S. Dhoot, A.J.A.B. Seeley, M.S. Khan, A. Köhler, R.H. Friend, Nature (London) 413 (2001) 828;
(b) W. Lu, B.-X. Mi, M.C.W. Chan, Z. Hui, C.-M. Che, N. Zhu, S.-T. Lee, J. Am. Chem. Soc. 126 (2004) 4958;
(c) C. Adachi, M.A. Baldo, M.E. Thompson, S.R. Forrest, J. Appl. Lett. 90 (2001) 5048;
(d) A. Tsuboyama, H. Iwawaki, M. Furugori, T. Mukaide, J. Kamatani, S. Igawa, T. Moriyama, S. Miura, T. Takiguchi, S. Okada, M. Hoshino, K. Ueno, J. Am. Chem. Soc. 125 (2003) 12971;
(e) M.K. Nazeeruddin, R. Humphry-Baker, D. Berner, S. Rivier, L. Zuppiroli, M. Graetzel, J. Am. Chem. Soc. 125 (2003) 8790;
(f) X. Gong, J.C. Ostrowski, G.C. Bazan, D. Moses, A.J. Heeger, M.S. Liu, A.K.-Y. Jen, Adv. Mater. 15 (2003) 45;
(g) A.S. Dhoot, N.C. Greenham, Adv. Mater. 14 (2002) 1834;
(h) P.K.H. Ho, J.S. Kim, J.H. Burroughes, H. Becker, S.F.Y. Li, T.M. Brown, F. Cacialli, R.H. Friend, Nature (London) 404 (2000) 481;
(i) Y. Cao, I.D. Parker, G. Yu, C. Zhang, A.J. Heeger, Nature (London) 397 (1999) 414;
(j) V. Cleave, G. Yahioglu, P. Le Barny, R.H. Friend, N. Tessler, Adv. Mater. 11 (1999) 285;
(k) M.A. Baldo, D.F. O'Brien, Y. You, A. Shoustikov, S. Sibley, M.E. Thompson, S.R. Forrest, Nature (London) 395 (1998) 151;
(l) M.A. Baldo, M.E. Thompson, S.R. Forrest, Nature (London) 403 (2000) 750;
(m) S.-C. Chan, M.C.W. Chan, Y. Wang, C.-M. Che, K.-K. Cheung, N. Zhu, Chem. Eur. J. 7 (2001) 4180.

[8] (a) N.J. Long, C.K. Williams, Angew. Chem. Int. Ed. 42 (2003) 2586;
(b) P. Nguyen, P. Gómez-Elipe, I. Manners, Chem. Rev. 99 (1999) 1515.

[9] (a) J.S. Wilson, N. Chawdhury, M.R.A. Al-Mandhary, M. Younus, M.S. Khan, P.R. Raithby, A. Köhler, R.H. Friend, J. Am. Chem. Soc. 123 (2001) 9412;
(b) M.S. Khan, M.R.A. Al-Mandhary, M.K. Al-Suti, B. Ahrens, M.F. Mahon, L. Male, P.R. Raithby, C.E. Boothby, A. Köhler, Dalton Trans. (2003) 74;
(c) M.S. Khan, M.R.A. Al-Mandhary, M.K. Al-Suti, A.K. Hisahm, P.R. Raithby, B. Ahrens, M.F. Mahon, L. Male, E.A. Marseglia, E. Tedesco, R.H. Friend, A. Köhler, N. Feeder, S.J. Teat, J. Chem. Soc., Dalton Trans. (2002) 1358;
(d) J.S. Wilson, A. Köhler, R.H. Friend, M.K. Al-Suti, M.R.A. Al-Mandhary, M.S. Khan, P.R. Raithby, J. Chem. Phys. 113 (2000) 7627;

(e) N. Chawdhury, A. Köhler, R.H. Friend, M. Younus, N.J. Long, P.R. Raithby, J. Lewis, Macromolecules 31 (1998) 722;
(f) W.-Y. Wong, C.-K. Wong, G.-L. Lu, A.W.-M. Lee, K.-W. Cheah, J.-X. Shi, Macromolecules 36 (2003) 983;
(g) W.-Y. Wong, G.-L. Lu, K.-H. Choi, J.-X. Shi, Macromolecules 35 (2002) 3506;
(h) W.-Y. Wong, K.-H. Choi, G.-L. Lu, Macromol. Rapid Commun. 22 (2001) 461;
(i) W.-Y. Wong, L. Liu, S.-Y. Poon, K.-H. Choi, K.-W. Cheah, J.-X. Shi, Macromolecules 37 (2004) 4496;
(j) W.-Y. Wong, S.-Y. Poon, A.W.-M. Lee, J.-X. Shi, K.-W. Cheah, Chem. Commun. (2004) 2420;
(k) S. Szafert, J.A. Gladysz, Chem. Rev. 103 (2003) 4175, and references therein;
(l) V.W.W. Yam, Acc. Chem. Res. 35 (2002) 555, and references therein;
(m) E.E. Silverman, T. Cardolaccia, X. Zhao, K.-Y. Kim, K. Haskins-Glusac, K.S. Schanze, Coord. Chem. Rev. (in press).

[10] (a) H.-Y. Chao, W. Lu, Y. Li, M.C.W. Chan, C.-M. Che, K.-K. Cheung, N. Zhu, J. Am. Chem. Soc. 124 (2002) 14696;
(b) W. Lu, H.-F. Xiang, N. Zhu, C.-M. Che, Organometallics 21 (2002) 2343;
(c) C.-M. Che, H.-Y. Chao, V.M. Miskowski, Y. Li, K.-K. Cheung, J. Am. Chem. Soc. 123 (2001) 4985;
(d) W.-Y. Wong, L. Liu, J.-X. Shi, Angew. Chem. Int. Ed. 42 (2003) 4064.

[11] (a) W.-Y. Wong, K.-H. Choi, G.-L. Lu, Z. Lin, Organometallics 21 (2002) 4475;
(b) W.-Y. Wong, K.-H. Choi, G.-L. Lu, J.-X. Shi, P.-Y. Lai, S.-M. Chan, Z. Lin, Organometallics 20 (2001) 5446.

[12] B. Li, B. Ahrens, K.-H. Choi, M.S. Khan, P.R. Raithby, P.J. Wilson, W.-Y. Wong, Cryst. Eng. Commun. 4 (2002) 405.

[13] (a) W.-Y. Wong, S.-M. Chan, K.-H. Choi, K.-W. Cheah, W.-K. Chan, Macromol. Rapid Commun. 21 (2000) 453;
(b) J. Lewis, P.R. Raithby, W.-Y. Wong, J. Organomet. Chem. 556 (1998) 219;
(c) W.-Y. Wong, W.-K. Wong, P.R. Raithby, J. Chem. Soc., Dalton Trans. (1998) 2761.

[14] (a) E. Gutierrez-Puebla, A. Vegas, S. Garcia-Blanco, Cryst. Struct. Commun. 8 (1979) 861;
(b) E. Gutierrez-Puebla, A. Vegas, S. Garcia-Blanco, Acta Crystallogr., Sect. B 34 (1978) 3382;
(c) B.F. Hoskins, R. Robson, E.E. Sutherland, J. Organomet. Chem. 515 (1996) 259;
(d) C. Hartbaum, G. Roth, H. Fischer, Eur. J. Inorg. Chem. (1998) 191;
(e) I. Ghosh, R. Mishra, D. Poddar, A.K. Mukherjee, Chem. Commun. (1996) 435.

[15] (a) N.W. Alcock, P.A. Lampe, P. Moore, J. Chem. Soc., Dalton Trans. (1980) 1471;
(b) C.A. Ghilardi, S. Midollini, A. Orlandini, A. Vacca, J. Chem. Soc., Dalton Trans. (1993) 3117.

[16] (a) R.J. Puddephatt, Chem. Commun. (1998) 1055, and references cited therein;
(b) R.J. Puddephatt, Coord. Chem. Rev. 216–217 (2001) 313;
(c) H. Schmidbaur, Nature 413 (2001) 31, and references cited therein.

[17] (a) S.J. Faville, W. Henderson, T.J. Mathieson, B.K. Nicholson, J. Organomet. Chem. 580 (1999) 363;
(b) W.-Y. Wong, G.-L. Lu, L. Liu, J.-X. Shi, Z. Lin, Eur. J. Inorg. Chem. (2004) 2066;
(c) X. Wang, L. Andrews, Inorg. Chem. 43 (2004) 7146.

[18] (a) P. Pyykko, Chem. Rev. 97 (1997) 597, and references cited therein;
(b) K.R. Flower, V.J. Howard, S. Naguthney, R.G. Pritchard, J.E. Warren, A.T. McGown, Inorg. Chem. 41 (2002) 1907;
(c) S.S. Batsanov, J. Chem. Soc., Dalton Trans. (1998) 1541.

[19] A. Bondi, J. Phys. Chem. 68 (1964) 441.

[20] (a) D. Rais, D.M.P. Mingos, R. Vilar, A.J.P. White, D.J. Williams, Organometallics 19 (2000) 5209;
(b) P.W.R. Corfield, H.M.M. Shearer, Acta Crystallogr. 20 (1966) 502;
(c) C. Brasse, P.R. Raithby, M.-A. Rennie, C.A. Russell, A. Steiner, D.S. Wright, Organometallics 15 (1996) 639.

[21] (a) I. Manners, Synthetic Metal-containing Polymers, Wiley-VCH, Weinheim, 2004 (Chapter 5, p. 165);
(b) N. Hagihara, K. Sonogashira, S. Takahashi, Adv. Polym. Sci. 41 (1981) 149.

[22] U.H.F. Bunz, Chem. Rev. 100 (2000) 1605.

[23] (a) D. Hertel, S. Setayesh, H.G. Nothofer, U. Scherf, K. Mullen, H. Bässler, Adv. Mater. 13 (2001) 65;
(b) A.P. Monkamn, H.D. Burrows, L.J. Hartwell, L.E. Horsburgh, I. Hamblett, S. Navaratnam, Phys. Rev. Lett. 86 (2001) 1358;
(c) Y.V. Romanovskii, A. Gerhard, B. Schweitzer, U. Scherf, R.I. Personov, H. Bässler, Phys. Rev. Lett. 84 (2000) 1027.

[24] D. Beljonne, H.F. Wittmann, A. Köhler, S. Graham, M. Younus, J. Lewis, P.R. Raithby, M.S. Khan, R.H. Friend, J.L. Brédas, J. Chem. Phys. 105 (1996) 3868.

[25] (a) S.D. Cummings, R. Eisenberg, J. Am. Chem. Soc. 118 (1996) 1949;
(b) H.F. Wittmann, R.H. Friend, M.S. Khan, J. Lewis, J. Chem. Phys. 101 (1994) 2693;
(c) N.J. Demas, G.A. Crosby, J. Am. Chem. Soc. 92 (1970) 7262.

[26] N.J. Turro, Modern Molecular Photochemistry, University Science Books, Mill Valley, CA, 1991.

[27] M.V. Russo, C. Lo Sterzo, P. Franceschini, G. Biagini, A. Furlani, J. Organomet. Chem. 619 (2001) 49.

[28] J. Chatt, B.L. Shaw, J. Chem. Soc. (1960) 4020.

[29] G.B. Kauffman, L.A. Teter, Inorg. Synth. 7 (1963) 245.

[30] SAINT+, ver. 6.02a, Bruker Analytical X-ray System, Inc., Madison, WI, 1998.

[31] G.M. Sheldrick, SADABS, Empirical Absorption Correction Program, University of Göttingen, Germany, 1997.

[32] G.M. Sheldrick, SHELXTL™, Reference Manual, ver. 5.1, Madison, WI, 1997.